Vibrationally Resolved Photoelectron Spectroscopy of Di-Gold Carbonyl Clusters Au-2(CO)(n)(-) (n=1-3): Experiment and Theory

5 AUTHORS, INCLUDING:

Jun Li
Tsinghua University
283 PUBLICATIONS **8,929** CITATIONS

SEE PROFILE

Lai-Sheng Wang
Brown University
434 PUBLICATIONS **18,876** CITATIONS

SEE PROFILE

Vibrationally Resolved Photoelectron Spectroscopy of Di-Gold Carbonyl Clusters Au$_2$(CO)$_n^-$ ($n = 1-3$): Experiment and Theory[†]

Yi-Lei Wang,[‡] Hua-Jin Zhai,[§] Lu Xu,[‡] Jun Li,*[,‡] and Lai-Sheng Wang*[,§,||]

Department of Chemistry & Key Laboratory of Organic Optoelectronics and Molecular Engineering of Ministry of Education, Tsinghua University, Beijing 100084, China, Department of Physics, Washington State University, 2710 University Drive, Richland, Washington 99354, and Chemical & Materials Sciences Division, Pacific Northwest National Laboratory, MS K8-88, P.O. Box 999, Richland, Washington 99352

We report vibrationally resolved photoelectron spectroscopy (PES) of Au$_2$(CO)$_n^-$ ($n = 1-3$), in combination with relativistic density functional theory (DFT) and ab initio calculations. The ground-state transition in the spectrum of Au$_2$CO$^-$ is broad, containing vibrational structures both in the bending and in the CO stretching modes and suggesting a large structural change from Au$_2$CO$^-$ to Au$_2$CO. The ground-state transitions for both $n = 2$ and 3 display a well-resolved vibrational progression in the CO stretching mode with frequencies of 2110 ± 40 and 2160 ± 40 cm^{-1}, respectively. The PES data show that chemisorption of the first two CO's each induces a significant red-shift in the electron binding energies. The third CO is physisorbed, inducing only a slight increase in electron binding energies relative to Au$_2$(CO)$_2^-$. Relativistic DFT and ab initio calculations are performed to determine the ground-state structures for Au$_2$(CO)$_n^-$ and Au$_2$(CO)$_n$, and the results agree well with the experiment. Au$_2$(CO), Au$_2$(CO)$_2$, and Au$_2$(CO)$_2^-$ are all found to be linear, while Au$_2$(CO)$^-$ is bent due to the Renner−Teller effect. A strong spin−orbit effect is found in Au$_2$(CO)$_2^-$ that quenches the Renner−Teller effect, keeping the linear structure for this anion. The physisorption in Au$_2$(CO)$_3^-$ is borne out in CCSD(T) calculations. However, a wide range of DFT methods tested fail to correctly predict the relative energies of the physisorbed versus chemisorbed isomers for Au$_2$(CO)$_3^-$.

1. Introduction

Catalysis of highly dispersed gold nanoparticles has been a rapidly expanding field since the pioneering work by Haruta and co-workers.[1] Despite extensive state-of-the-art surface investigations over the past 20 years,[2–18] the mechanisms of the highly useful catalytic reactions involving gold are not well understood.[1,19] Gas-phase studies of CO and O$_2$ adsorption on size-selected Au clusters have emerged as an alternative approach to provide insight into the mechanisms of catalytic CO oxidation.[20–49] Experimental and theoretical studies have established that O$_2$ adsorbs molecularly on certain gold clusters.[20–23] Coadsorption of CO and O$_2$ on small gold clusters was also observed, in which CO and O$_2$ were shown to adsorb cooperatively.[24,25]

The interaction of CO with gold clusters has been the subject of numerous studies, and saturation adsorption of CO on gold clusters has been observed.[24,29–37] Infrared spectra of Au−CO complexes in neon matrix have led to the identifications of AuCO, Au(CO)$_2$, Au$_2$(CO)$_2$, Au$_n$(CO) ($n = 2-5$), and Au(CO)$_n^+$ ($n = 1-4$).[31,34] Vibrational spectroscopy on size-elected Au$_m$(CO)$_n^+$ and Au$_m$(CO)$_n^-$ clusters has also been reported.[35,37] The adsorption energies of CO on gold cluster cations Au$_n^+$ ($n = 1-65$) have been determined in a radiative association kinetics study, ranging from 1.1 eV for smaller clusters to 0.65 eV for larger ones.[36] However, the electronic and structural properties of CO−Au$_n^-$ clusters remain poorly understood. We reported

previously photoelectron spectroscopy (PES) of several series of gold carbonyl cluster anions, Au$_m$(CO)$_n^-$ ($m = 2-5$, $n = 1-7$).[50] We observed that adsorption of the first few CO's induces significant red-shifts to the PES spectra. For each gold cluster, CO adsorption reaches a critical number, beyond which further CO adsorption hardly changes the spectra. The critical CO number corresponds exactly to the available low-coordinate apex sites in the corresponding bare Au clusters. We suggested that CO first chemisorbs to the apex sites and additional CO's only physisorb to the chemisorption-saturated Au−CO complexes. In subsequent studies on the Au$_6$(CO)$_n^-$ ($n = 1-9$) complexes,[51,52] we observed that the first three CO's chemisorb to the three apex sites of the triangular Au$_6^-$ cluster. Starting from the adsorption of the fourth CO, significant structural changes occur for the Au$_6^-$ cluster such that it can chemisorb up to six CO's, whereas additional CO's are physisorbed.

In the current Article, we report a combined experimental and theoretical study on a series of di-gold carbonyl clusters: Au$_2$(CO)$_n^-$ and Au$_2$(CO)$_n$ ($n = 1-3$). Higher resolution PES spectra are obtained at 532 nm (2.331 eV), yielding vibrational information and more accurate electron detachment energies. The adsorption of the first two CO's each decreases significantly the electron binding energies, whereas the third CO is physisorbed, inducing a slight increase in the electron binding energies. The ground-state detachment transitions are vibrationally resolved in the CO stretching mode with frequencies of 2110 ± 40 and 2160 ± 40 cm^{-1}, respectively, for Au$_2$(CO)$_2$ and Au$_2$(CO)$_3$. The CO frequency in Au$_2$(CO)$_2$ is substantially red-shifted with respect to bare CO (2143 cm^{-1}), while that in Au$_2$(CO)$_3$ is slightly blue-shifted. The latter is unexpected and may provide interesting insights into the nature of surface Au−CO species.[13,53–62] We have performed DFT and ab initio

* Corresponding author. E-mail: junli@tsinghua.edu.cn; ls.wang@pnl.gov.
‡ Tsinghua University.
§ Washington State University and Pacific Northwest National Laboratory.
|| Permanent address: Department of Chemistry, Brown University, 324 Brook Street, Providence, RI 02912.

calculations including scalar relativistic and spin−orbit (SO) coupling effects for $Au_2(CO)_n^-$ and $Au_2(CO)_n$. The ground state of $Au_2(CO)^-$ is found to be considerably bent with a Au−C−O bond angle of 133°, whereas $Au_2(CO)$ is linear. Both $Au_2(CO)_2^-$ and $Au_2(CO)_2$ are shown to be linear. All DFT methods used are shown to be inadequate for the $Au_2(CO)_3^-$ complex. Only CCSD(T) calculations predict the physisorbed $Au_2(CO)_3^-$ isomer to be the ground state, consistent with the experimental observation.

2. Experimental and Computational Methods

2.1. Photoelectron Spectroscopy. The experiment was carried out using a magnetic-bottle PES apparatus equipped with a laser vaporization supersonic cluster source, the details of which have been described elsewhere.[63] Briefly, the $Au_m(CO)_n^-$ cluster anions were produced by laser vaporization of a pure gold target in the presence of a helium carrier gas seeded with 2% CO. Various $Au_m(CO)_n^-$ clusters were generated and analyzed using a time-of-flight mass spectrometer. The $Au_2(CO)_n^-$ ($n = 0-3$) species of current interest were each mass-selected and decelerated before being photodetached. Under our experimental conditions, only relatively weak mass signals were observed for the $Au_2(CO)_n^-$ species, whereas no mass signals were observed for the $Au(CO)_n^-$ series. These observations suggest that Au^- and Au_2^- are probably less reactive with CO than the larger clusters, consistent with previous experiments on chemical reactivity of gold cluster anions.[21,24,30,33] PES spectra were measured at 532 nm (2.331 eV). Photoelectrons were collected at nearly 100% efficiency by the magnetic bottle and analyzed in a 3.5 m long electron flight tube. The PES spectra were calibrated using the known spectra of Rh^-, and the energy resolution of the apparatus was $\Delta E_k/E_k \approx 2.5\%$, that is, ∼25 meV for 1 eV electrons.

2.2. Computational Methods. DFT calculations were performed using the PW91 functional of the generalized gradient approximation (GGA) implemented in the Amsterdam Density Functional program (ADF 2007.01).[64] The uncontracted Slater basis sets with the quality of triple-ζ plus two polarization functions (TZ2P) were used, with the frozen core approximation applied to the $[1s^2-4f^{14}]$ core for Au and the $[1s^2]$ cores for both C and O.[65] The scalar relativistic (SR) and SO coupling effects were taken into account by the zero-order-regular approximation (ZORA).[66] Geometries were optimized at the SR level, and single-point energy calculations were performed at the SO level. Vibrational frequency calculations were carried out to verify that the species are minima on the potential energy surface. Vertical electron detachment energies (VDEs) were obtained at the anion geometry by using a combined ΔSCF-TDDFT approach,[67] where the first VDE was calculated from the difference of the ground-state energy of the anions and neutrals (i.e., ΔSCF) and the higher VDEs were calculated from the ground-state energy of the anions and the excited-state energies of the neutrals by using TDDFT. To better describe the neutral excited states, the SAOP (statistical average of orbital potentials) functional was also used to do TDDFT calculations, where all-electron basis sets were applied for all of the atoms.

Because of the complicated nature of the delicate electron correlations in the gold and CO interactions,[41] ab initio wave function theory calculations at the coupled-cluster level with single and double and perturbative triple excitations [CCSD(T)][68] were also performed for $n = 0-2$ using the MOLPRO 2008 program[69] to assess the accuracy of the DFT results. We used a relativistic 19-valence-electron pseudopotential (ECP60MDF)[70] and the aug-cc-pVTZ-PP basis sets[71] (11s10p9d3f2g)/[6s6p5d3f2g] for gold and

aug-cc-pVTZ basis sets for carbon and oxygen,[72] denoted as AVTZ hereafter. The SO coupling effect was included by using a state-interacting method[73] with spin−orbit pseudopotentials at the complete active space self-consistent field (CASSCF)[74] level of theory, and SO-free energies were replaced by those from CCSD(T) calculations. Because the proper selection of active spaces is crucial to state-averaged CASSCF calculations, we included all of the 5d and 6s orbitals for Au_2 in the active space with all 22 electrons in 12 active orbitals being correlated, that is, CASSCF(22e, 12o). For $Au_2(CO)$ and $Au_2(CO)_2$, large-size active spaces including the 5d and 6s orbitals of Au and the frontier π and π^* orbitals of CO were adopted, that is, CASSCF(26e, 16o) for $Au_2(CO)$ and CASSCF(30e, 19o) for $Au_2(CO)_2$. Based on the contributions of the orbitals in these active spaces to the concerned states, the following spaces were chosen to reduce the computational cost of the subsequent calculations: CASSCF(6e, 6o) for $Au_2(CO)$ and CASSCF(18e, 13o) for $Au_2(CO)_2$. The occupations of the natural orbitals agree with each other within 0.01 and 0.002, respectively, for $Au_2(CO)$ and $Au_2(CO)_2$ between the two types of active spaces. Additionally, the first excited energies calculated using the two types of active spaces are the same for $Au_2(CO)$, indicating the smaller active space is appropriate. The states relevant to the first excitation were included in the state-averaged CASSCF, with the following states being selected on the basis of our TDDFT results: $^1\Sigma_g$, $^3\Pi_u$, and $^3\Sigma_u$ for Au_2, $^1A'$ and $^3A'$ for $Au_2(CO)$, and $^1\Sigma_g$ and $^3\Pi_u$ for $Au_2(CO)_2$.

Because the PW91 method turned out to have large errors for $Au_2(CO)_3^-$, we further performed DFT calculations using hybrid functionals of B3LYP and TPSSh, and GGA functional of PW91, using the NWChem 5.0 program.[75] On the basis of the optimized TPSSh geometries, ab initio calculations were further carried out at the CCSD(T) level using MOLPRO 2008. In these calculations, we used the same AVTZ basis sets as before. Basis sets superposition error (BSSE) was corrected with the counterpoise method[76] using Au_2^- and CO's as fragments.

3. Experimental Results

The PES spectra of $Au_2(CO)_n^-$ ($n = 0-3$) at two detachment photon energies are shown in Figure 1. The 193 nm spectra (Figure 1a), which revealed more electronic transitions, were reported previously[50] and are included here for comparison with the 532 nm data and the theoretical calculations. The main observations from the 193 nm data were that the first two CO's each induce a significant red-shift for the electron binding energies of the ground-state transition (X) by ∼0.5−0.7 eV, whereas the third CO induces a slight blue-shift (0.17 eV) (Table 1). The second PES band (A) was observed at roughly constant binding energies (3.9−4.2 eV), causing the X−A energy gaps (i.e., the HOMO−LUMO gaps of the corresponding neutral clusters) to increase as a function of CO from $2.00 \rightarrow 2.55 \rightarrow 3.26 \rightarrow 3.35$ eV for $Au_2(CO)_n^-$ ($n = 0-3$) (Table 1).

The 532 nm spectra (Figure 1b) only allowed the ground-state transition to be observed and were significantly better resolved with vibrational structures in each case. We reported the 532 nm spectrum of Au_2^- in our previous study of Au_2H^-.[77] It displays a vibrational progression with a spacing of 190 ± 15 cm^{-1}, which agrees with a prior high resolution spectrum.[78] The $Au_2(CO)^-$ spectrum appears to be rather broad, and vibrational structures were not well resolved except for a hint of the $1 \leftarrow 0$ transition for CO stretching at ∼1.75 eV. The broad spectrum indicates a large anion-to-neutral structure change and the involvement of multiple vibrational modes. Thus, the adiabatic electron detachment energy (ADE) for $Au_2(CO)^-$
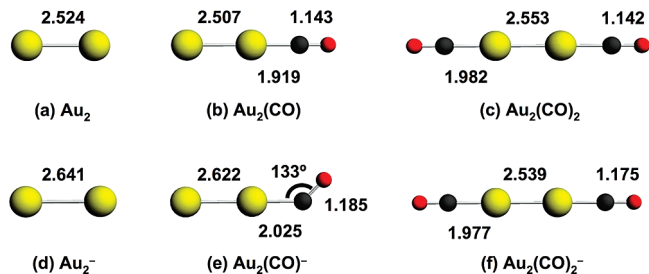
Di-Gold Carbonyl Clusters $Au_2(CO)_n^-$ ($n = 1-3$)

J. Phys. Chem. A, Vol. 114, No. 3, 2010 **1249**
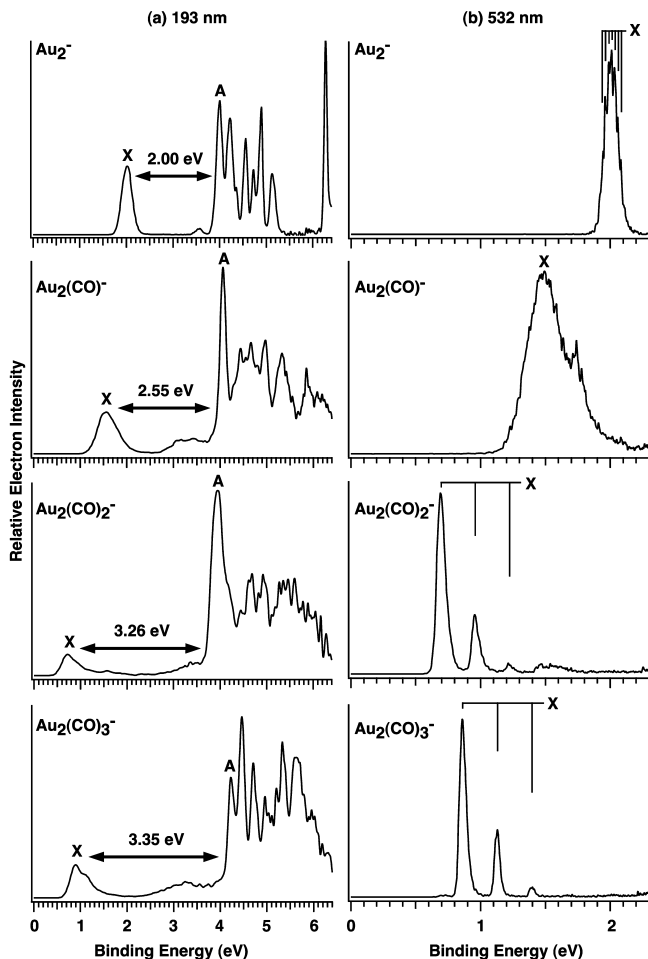
Figure 1. Photoelectron spectra of $Au_2(CO)_n^-$ ($n = 0-3$) at (a) 193 nm (6.424 eV) and (b) 532 nm (2.331 eV). Energy gaps between features X and A for each species are labeled. Vertical bars indicate the resolved vibrational structures.

Figure 2. Optimized structures of $Au_2(CO)_n$ and $Au_2(CO)_n^-$ ($n = 0-2$) at the DFT/PW91 level. Bond lengths are in angstroms.
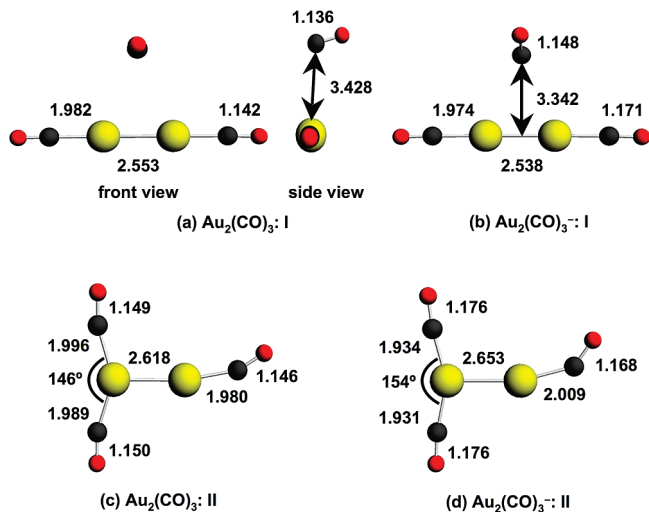
Figure 3. Optimized structures of $Au_2(CO)_3$ and $Au_2(CO)_3^-$ at the DFT/PW91 level. Bond lengths are in angstroms.

TABLE 1: Observed Adiabatic (ADE) and Vertical (VDE) Detachment Energies, Energy Gaps, and Vibrational Frequencies from the Photoelectron Spectra of $Au_2(CO)_n^-$ ($n = 0-3$)

			VDE (eV)[a]			
	ADE (eV)[a]	ΔADE (eV)[b]	band X	band A	X−A gap (eV)[c]	vib. freq. (cm⁻¹)[a,d]
Au_2^-	1.94 (2)[e]		2.01 (2)	4.01 (2)	2.00	190 (15)[e]
$Au_2(CO)^-$	1.25 (5)[f]	−0.69	1.50 (3)	4.05 (2)	2.55	
$Au_2(CO)_2^-$	0.69 (3)	−0.56	0.69 (3)	3.95 (3)	3.26	2110 (40)
$Au_2(CO)_3^-$	0.86 (3)	0.17	0.86 (3)	4.21 (2)	3.35	2160 (40)

[a] Numbers in parentheses represent experimental uncertainties in the last digits. [b] ΔADE $\equiv$ ADE [$Au_2(CO)_n^-$] − ADE [$Au_2(CO)_{n-1}^-$], which characterizes the influence of the nth CO molecule to the electron binding energies of $Au_2(CO)_n^-$. [c] Evaluated from the VDE difference between bands X and A. [d] Ground-state vibrational frequencies of the corresponding neutral species. [e] More accurate ADE (1.938 ± 0.007 eV) and vibrational frequency (190.9 cm⁻¹) were reported previously (ref 78). [f] Because of the large geometry change between the anion and neutral, this number should be considered as a threshold value, which represents the upper limit of the true ADE.

(1.25 eV, Table 1) estimated from the leading edge of the broad spectrum should be considered as a threshold value, which represents the upper limit for the true ADE. In contrast, the spectra of $Au_2(CO)_2^-$ and $Au_2(CO)_3^-$ each exhibit a well-resolved vibrational progression with spacings of 2110 ± 40

and 2160 ± 40 cm⁻¹, respectively, which should correspond to the CO stretch. The ADE and VDE for both the $n = 2$ and 3 species can be accurately determined from the intense and sharp 0−0 peak in the corresponding spectrum, as given in Table 1.

The weak broad feature at ~1.5 eV in the 532 nm spectrum of $Au_2(CO)_2^-$ (Figure 1b), which is also discernible in the 193 nm (Figure 1a), has binding energies similar to the spectrum of $Au_2(CO)^-$. It is likely due to photofragmentation, $Au_2(CO)_2^- + h\nu \rightarrow Au_2(CO)^- + CO$, followed by photodetachment of the $Au_2(CO)^-$ product. The weak feature at ~3.6 eV in the 193 nm spectrum of Au_2^- (Figure 1a) was identified to come from the Au_2H^- impurity previously.[77] There are also visible weak features between the X and A bands in the 193 nm spectra of $Au_2(CO)_n^-$ ($n = 1-3$), which were likely due to minor impurities.

4. Theoretical Results

The optimized structures at PW91 level are shown in Figure 2 for $Au_2(CO)_n^-$ and $Au_2(CO)_n$ ($n = 0-2$), and those for $n = 3$ are in Figure 3. We calculated a variety of possible geometries for $Au_2(CO)^-$, $Au_2(CO)_2^-$, and their neutrals. In the lowest energy structures, CO is found to coordinate to Au_2 terminally via the C atom. The lowest energy structure of $Au_2(CO)^-$ (²A′, Figure 2e) is bent with C_s symmetry, whereas $Au_2(CO)_2^-$ (²Π$_u$, Figure 2f) is linear with $D_{\infty h}$ symmetry. Both $Au_2(CO)$ (¹Σ) and $Au_2(CO)_2$ (¹Σ$_g$) neutrals are linear with $C_{\infty v}$ and $D_{\infty h}$ symmetries, respectively. Our result for the bent $Au_2(CO)^-$ agrees with several previous DFT calculations.[38−41] Our linear $Au_2(CO)$ structure also agrees with two previous calculations.[39,41]

For $Au_2(CO)_3^-$ and $Au_2(CO)_3$, we performed PW91 geometry optimizations on many possible structures including mixed

TABLE 2: Calculated PW91 Adiabatic (ADE) and Vertical (VDE) Detachment Energies and Energy Gaps for $Au_2(CO)_n^-$ ($n = 0-3$), and Vibrational Frequencies of the Corresponding Neutral Species[a]

| | ADE (eV) | ΔADE (eV)[b] | VDE (eV) | | X−A gap (eV) | | | vib. freq. (cm^{-1})[c] |
			feature X	feature A	PW91	SAOP	CCSD(T)	
Au_2^-	1.94		2.01	3.48	1.47	1.67	1.96	177
$Au_2(CO)^-$	1.19	−0.75	1.77	3.40	1.63	1.71	2.49	2093
$Au_2(CO)_2^-$	1.06	−0.13	1.17	3.73	2.56	2.45	3.23	2095
$Au_2(CO)_3^{-d}$	1.20	0.15	1.30	3.82	2.52			2095, 2119

[a] The X−A gaps at the SAOP and CCSD(T) levels are also included. All quantities were calculated with SO corrections except the vibrational frequencies, for which only scalar-relativistic effects were included. [b] See footnote b in Table 1. [c] Ground-state vibrational frequencies of the corresponding neutral species. For the CO complexes, the frequency refers to the CO stretch. [d] Isomer I (Figure 3b). The corresponding data for isomer II (Figure 3d): ADE (1.55 eV), VDE (1.74 eV), and X−A gap (1.24 eV).
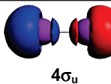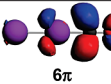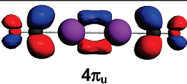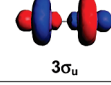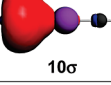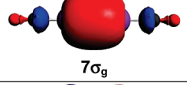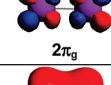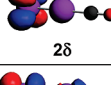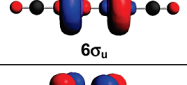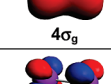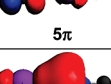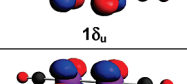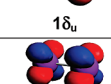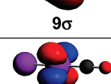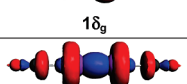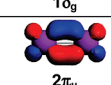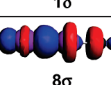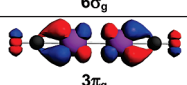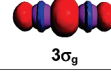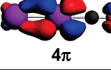
chemisorption−physisorption complexes and all-CO-chemisorbed structures. The two low-lying structures are shown in Figure 3, where isomer I of $Au_2(CO)_3^-$ (C_s, $^2A'$) contains a physisorbed CO lying aslant above the linear $Au_2(CO)_2^-$ core. In isomer II (C_s, $^2A''$), all three CO's are chemisorbed with one Au atom coordinated by two CO's. For the anions, PW91 calculations predict isomer II to be 0.48 eV lower in energy than isomer I. For the $Au_2(CO)_3$ neutral, PW91 predicts isomer II (C_s, $^1A''$) to be more stable than isomer I (C_s, $^1A'$) by 0.13 eV. However, the calculated VDEs and simulated PES spectrum from isomer II of $Au_2(CO)_3^-$ do not agree with the experiment (see footnote d in Table 2). Thus, further DFT and ab initio calculations were performed to evaluate the relative energies between isomers I and II for $Au_2(CO)_3^-$. With ZPE (zero-point energy) and SO corrections, the PW91, B3LYP, and TPSSh methods using the AVTZ basis sets erroneously predict that isomer II is lower in energy than isomer I by 0.46, 0.10, and 0.31 eV, respectively. While the BSSE correction is only 0.003 eV with TPSSh, it becomes as large as 0.16 eV with CCSD(T)/AVTZ. As a result, CCSD(T) single-point energy calculations with ZPE, BSSE, and SO corrections correctly predict that isomer I is lower in energy than isomer II by about 0.02 eV. Note that the two near-degenerate states of $Au_2(CO)_3^-$ (isomer I) derived from the $^2\Pi_u$ ground state of $Au_2(CO)_2^-$ are within 0.04 eV at the CCSD(T)/VTZ level of theory.

The adsorption energies of the first and second CO to Au_2^- are −1.03 and −0.94 eV, respectively. These adsorption energies reveal that the adsorption of the first CO does not prevent the adsorption of the second 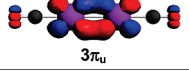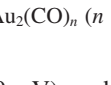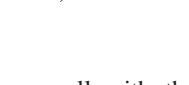CO and the first two CO's have similar binding strengths to those of the Au_2^- core. When the two terminal sites are used up, the third CO becomes physisorbed with a rather small adsorption energy of −0.19 eV. This theoretical result is consistent with our previous observation that CO prefers apex sites on small Au_n^- clusters.[50−52]

The calculated electronic properties for $Au_2(CO)_n^-$ and $Au_2(CO)_n$ at the PW91 level are summarized in Table 2. Apparently, PW91 underestimates the energy gaps by 0.5−0.9 eV. Such deviation is far larger than expected, prompting us to compute the energy gaps using the SAOP and CCSD(T) methods (Table 2). While the SAOP results show no improvement as compared to the PW91 data, the CCSD(T) results indeed agree well with the experiment.

5. Comparison between Experiment and Theory

As shown in Table 2, the PW91 ADE (1.94 eV) and the first VDE (2.01 eV) for Au_2^- are in quantitative agreement with the corresponding experimental values (Table 1). However, the PW91 VDE for the first excited band A (3.48 eV) is lower by 0.53 eV relative to the experimental value (4.01 eV), resulting in a much smaller PW91 X−A gap. For $Au_2(CO)^-$, the PW91

Figure 4. Contour surfaces (isosurface value = 0.04 au) of the frontier orbitals of $Au_2(CO)_n$ ($n = 0-2$).

ADE (1.19 eV) and VDE (1.77 eV) agree well with the experimental values (Table 1). Again, the PW91 VDE for band A (3.40 eV) is much lower relative to the experimental value (4.05 eV). For $Au_2(CO)_2^-$, the PW91 ADE (1.06 eV) and the first VDE (1.17 eV) are both too high relative to the experiment by 0.37 and 0.48 eV, respectively. For $Au_2(CO)_3^-$, the PW91 ADE (1.20 eV) and the first VDE (1.30 eV) for the physisorbed isomer (Figure 3b) are also too high, but the deviation (0.34 and 0.44 eV) relative to the experiment is similar to those for $Au_2(CO)_2^-$. However, the PW91 ADE and the first VDE for the chemisorbed isomer II (Figure 3d) totally disagree with the experiment (see footnote d in Table 2) and thus can be ruled out to be responsible for the observed spectra of $Au_2(CO)_3^-$.

As mentioned above, the PW91 VDE for the first excited state band A is all significantly underestimated, resulting in smaller X−A gaps for all $Au_2(CO)_n^-$ ($n = 1-3$) species. The deviation from experiment is −0.53 eV for Au_2^- and varies between −0.70 and −0.92 eV for $Au_2(CO)_n^-$ ($n = 1-3$). The valence molecular orbitals for neutral $Au_2(CO)_n$ ($n = 0-2$) are shown in Figure 4. The LUMO's for $Au_2(CO)$ and $Au_2(CO)_2$ are mainly CO π^* orbitals, and their HOMO's mainly involve a Au_2 σ orbital. The X−A gap is equivalent to promote a Au_2 σ electron to the CO π^* orbital, that is, a metal-to-ligand charge

transfer transition. It is known that TDDFT tends to underestimate excitation energies of charge-transfer transitions,[79] explaining why the errors of the PW91 X−A gaps for $Au_2(CO)_n^-$ ($n = 1-3$) are much more severe as compared to that for Au_2^-.

To further investigate the large PW91 deviations of the X−A gaps, CCSD(T) and SAOP calculations were performed for $Au_2(CO)_n$ ($n = 0-2$). $Au_2(CO)_3$ was omitted in these calculations because the nature of its electronic transition to the first excited state is similar to that of $Au_2(CO)_2$ due to the physisorbed nature of the third CO. The CCSD(T) X−A gaps are also shown in Table 2, and they are in quantitative agreement with the experiment. However, the overall performance of the asymptotically corrected SAOP (Table 2) functional is no better than PW91.

The structural changes between the anions and neutral CO-complexes are also consistent with the experimental observations. The $Au_2(CO)^-$ anion is bent with a ∠AuCO angle of 133° (Figure 2e), while the ground state of $Au_2(CO)$ is linear (Figure 2b), which explains the broad ground-state PES band. The CO bond length is also slightly shortened from $Au_2(CO)^-$ to $Au_2(CO)$ by 0.042 Å, consistent with the observation of CO stretch in the 532 nm spectrum (Figure 1b). The large difference between the calculated ADE and VDE for $Au_2(CO)^-$ reflects the large structural changes upon electron detachment. For $Au_2(CO)_2^-$ and the physisorbed $Au_2(CO)_3^-$, there is very little structure change upon electron detachment. The main difference is the slight shortening of the CO bond length, consistent with the simple CO stretching progression observed in the 532 nm spectra of $Au_2(CO)_2^-$ and $Au_2(CO)_3^-$ (Figure 1b). Again, the difference between the calculated ADE and VDE for $Au_2(CO)_2^-$ and $Au_2(CO)_3^-$ is also very small, in line with the small structural change upon electron detachment. The simple CO vibrational progression observed in the 532 nm spectrum of $Au_2(CO)_3^-$ can also rule out the chemisorbed isomer II because there are more significant structural changes between the anion and the neutral (Figure 3c and d). The calculated CO stretching frequencies for $Au_2(CO)_n$ at the PW91 level are 2093 cm^{-1} for $n = 1$, 2095 cm^{-1} for $n = 2$, and 2095 and 2119 cm^{-1} for $n = 3$ (Table 2). Considering the complexity of the Au−CO system,[13,80,81] the agreement between the computed and experimental frequencies is reasonable.

Overall, the theoretical results are in good agreement with the experiment, lending considerable credence to the structures identified for $Au_2(CO)_n^-$ and $Au_2(CO)_n$ ($n = 1-3$).

6. Discussion

6.1. $Au_2(CO)^-$ and $Au_2(CO)_2^-$: Renner−Teller Effect versus Spin−Orbit Effect.
The decrease of electron binding energies upon CO chemisorption to Au_2^- in the $Au_2(CO)_n^-$ ($n = 1-2$) complexes is quite unusual, suggesting strong chemical interactions. The molecular orbitals shown in Figure 4 allow a qualitative understanding of this trend. The LUMO of Au_2 is an antibonding σ orbital. The terminal coordination of CO to Au_2 in the linear complexes would significantly destabilize this orbital. Consequently, the LUMO's of $Au_2(CO)$ and $Au_2(CO)_2$ become the unoccupied CO π* orbitals, which are much higher lying relative to the LUMO of Au_2. Occupation of these high lying CO-centered LUMO's by the extra electron in the $Au_2(CO)_n^-$ anions would result in reduced electron binding energies relative to the bare Au_2^-.

In the linear structure, occupation of the doubly degenerate LUMO would lead to doubly degenerate electronic states: $^2\Pi$ for $Au_2(CO)^-$ and $^2\Pi_u$ for $Au_2(CO)_2^-$. In these linear anions, the degenerate electronic states are unstable against bending

vibrations, resulting in the Renner−Teller (RT) effect that would distort the linear structures and lift the electronic degeneracy.[82] The RT effect is similar to the Jahn−Teller effect for nonlinear molecules. The bent structure of $Au_2(CO)^-$ is entirely a consequence of the RT effect. However, the RT effect does not seem to occur in $Au_2(CO)_2^-$: our optimized structure for this anion with SO effect remains linear, in agreement with the simple vibrational progression in the 532 nm PES spectrum. Our analysis showed that the $4\pi_u$ LUMO of $Au_2(CO)_2$ contains 19% Au 6p and 3% Au 5d characters, leading to a SO splitting energy of 0.20 eV, which is larger than the RT effect (0.16 eV). Thus, the RT effect is quenched and the anion remains linear as a result of the strong SO effect. A similar analysis revealed that the 6π LUMO orbital of $Au_2(CO)$ contains 15% Au 6p and 8% Au 5d character. Because the Au 6p orbitals have a large SO effect, less Au 6p character results in less SO splitting (0.09 eV) for $Au_2(CO)^-$ as compared to $Au_2(CO)_2^-$ (0.20 eV). The calculated RT energy is 0.67 eV for $Au_2(CO)^-$, much larger than the SO splitting energy for $Au_2(CO)^-$. Hence, the RT effect dominates in $Au_2(CO)^-$, leading to the bent structure. There is a previous report of a bent $Au_2(CO)_2^-$,[40] which is problematic because of the neglect of the SO effect.

It is noteworthy that in the bent $Au_2(CO)^-$ structure the singly occupied orbital has weaker σ-donation from CO and a considerable Au−Au σ* character like in the Au_2^- anion. Consequently, the Au−Au bond lengths in these two anions are both lengthened by more than 0.1 Å as compared to the corresponding neutrals. On the contrary, in $Au_2(CO)_2^-$ the excess electron is located in the neutral LUMO, which has a small σ-bonding character between the two gold atoms due to the $D_{\infty h}$ symmetry. Therefore, the Au−Au bond length of the $Au_2(CO)_2^-$ anion is smaller than that of the neutral by 0.014 Å.

6.2. Comparison between DFT and ab Initio Methods for $Au_2(CO)_3^-$: Physisorption versus Chemisorption.
The experimental PES spectra of $Au_2(CO)_3^-$ are similar to those of $Au_2(CO)_2^-$ (Figure 1), suggesting that the third CO in $Au_2(CO)_3^-$ is physisorbed to a $Au_2(CO)_2^-$ core. However, at the PW91 level of theory, the chemisorbed isomer II (Figure 3d) is predicted to be the lowest in energy for $Au_2(CO)_3^-$, but its calculated first VDE (1.74 eV), second VDE (2.98 eV), and energy gap (1.24 eV) deviate considerably from the experiment (first VDE, 0.86 eV; second VDE, 4.21 eV; energy gap, 3.35 eV). Furthermore, one of the Au atoms in this isomer is coordinated by two CO ligands, which is inconsistent with the general observation that each low-coordinate Au atom can only chemisorb one CO ligand at low CO coverage.[50−52] It is known that DFT methods can carry large errors in predicting relative energies of isomers with significantly different geometries or physiochemical interactions.[83] Indeed, single-point CCSD(T) calculations show that the physisorbed isomer I is more stable by ∼0.02 eV, suggesting the PW91 calculations carry a large error (at least 0.5 eV) for the relative energies for the $Au_2(CO)_3^-$ isomers. This is not totally surprising considering the complicated nature of Au−CO interactions and the weak interactions involving the physisorbed CO. We also note that the popular B3LYP, PW91, and TPSSh methods with SO corrections also incorrectly predict that isomer II is 0.10, 0.46, and 0.31 eV, respectively, lower in energy.

In isomer I of $Au_2(CO)_3^-$ (Figure 3b), the distance between the C atom of the physisorbed CO and the middle point of the two Au atoms is 3.342 Å, and the C···Au distance is 3.575 Å. This C···Au distance is much larger than the sum of the atomic radius, indicating only weak van der Waals interactions between

the third CO and Au_2. Treating such weak interactions is still a challenging bottleneck for DFT methods, suggesting the importance of accurate experimental data and the interplay of combined experimental and theoretical efforts.

6.3. $Au_2(CO)_2$ and $Au_2(CO)_3$: Classical versus Nonclassical Au(0)−CO Complexes. The 532 nm spectra of $Au_2(CO)_2^-$ and $Au_2(CO)_3^-$ (Figure 1b) represent the only species for which it is possible to resolve a CO stretching progression among all $Au_m(CO)_n^-$ ($m = 2−6$; $n = 1−9$) complexes that we have investigated.[50−52] Relative to free CO molecule (vibrational frequency: 2143 cm^{-1}), the vibrational frequency of $Au_2(CO)_2$ (2110 cm^{-1}) is red-shifted, making the $Au_2(CO)_2$ complex a "classical" carbonyl species. In contrast, the vibrational frequency of $Au_2(CO)_3$ (2160 cm^{-1}) is slightly blue-shifted relative to free CO, making it a "nonclassical" carbonyl species.[37,84]

Chemical bonding in transition metal carbonyl complexes (M−CO) comprises M←CO σ donation and M→CO π back-donation: CO is both a σ-donor and a π-acceptor ligand.[84] The CO stretching frequency is a useful indicator of the magnitude of σ- and π-bonding in metal carbonyls. In classical M−CO transition metal complexes, strong M→CO π back-donation weakens the CO bond, resulting in a red-shift in the CO stretching frequency. However, strong σ donation or weak π back-donation can lead to stronger CO bonding and an increased CO stretching frequency in nonclassical M−CO complexes. Surface studies show that CO stretching in Au(0)−CO species is at ~2110 cm^{-1},[53−62] where the red-shift relative to free CO molecule is small. Our current observation of a CO stretching frequency of 2110 cm^{-1} in $Au_2(CO)_2$ is in excellent agreement with the surface results. Our observed CO stretching in $Au_2(CO)_2$ falls between those observed for $Au_m(CO)_n^+$ and $Au_m(CO)_n^-$ from gas-phase IR spectroscopy.[35]

Au−CO complexes are rare, but it is generally believed that σ donation is important in Au−CO complexes, whereas π back-donation is negligible, making them nonclassical carbonyl complexes. This usually involves a Au^+ center.[37,84] However, a nonclassical Au(0)−CO species has not been reported in the literature.[31,34,53−62] The $Au_2(CO)_3$ complex represents an example of nonclassical Au(0)−CO species. Although our measured frequencies (2160 cm^{-1}) carry large uncertainties, the relatively large CO vibrational spacing in the 532 nm spectrum of $Au_2(CO)_3^-$ in comparison to that of $Au_2(CO)_2^-$ is quite obvious (Figure 1b). The CO stretching frequencies in $Au_2(CO)_2$ and $Au_2(CO)_3$ differ by as large as 50 cm^{-1}, despite the fact that the third CO in $Au_2(CO)_3^-$ and $Au_2(CO)_3$ is shown to interact weakly with the chemisorbed $Au_2(CO)_2$ core (Figure 3a and b), suggesting that the weakly bonded CO influences the interactions of the terminal CO with gold. As shown in Figure 3a, the physisorbed CO is in a bridging position and weakly interacts with both Au atoms. It is conceivable that the weak CO−Au_2 interactions withdraw net charge from the Au_2 core, thus strengthening the CO→Au σ donation and weakening the Au→CO π back-donation for the terminal CO's.

The active Au species in gold catalysts have been assigned on the basis of the observed CO frequencies as follows: Au(0)−CO (2105−2120 cm^{-1}), $Au^{\delta+}$−CO (2130, 2145 cm^{-1}), Au(I)−CO (2160−2170 cm^{-1}), and Au(III)−CO (>2170 cm^{-1}).[13,54−62] However, two recent benchmarking theoretical works on the simplest AuCO complex[41,81] showed the complexity of the Au−CO system, suggesting that the equilibrium geometry, the adsorption energies, and in particular the CO vibrational frequency are all challenging properties to calculate for the current approximate methods. In this context, gas-phase vibrational information such as that obtained from the current

study is valuable both in helping resolve the controversy in surface studies and in calibrating the computational methods. For example, numerous surface studies have shown Au carbonyl species with CO frequencies between 2150 and 2170 cm^{-1}, and their assignments have been inconsistent and controversial.[54−58] Freund and co-workers[57] reported an intriguing surface carbonyl species at 2165 cm^{-1}, which appeared at higher or saturated CO exposure. It corresponds to a more weakly bound CO relative to those on Au(0) sites and is assigned to CO bound to extremely small Au clusters with Au^+ character, inconsistent with the common notion that cationic Au absorbs CO more strongly. In light of our current observation, it is conceivable that nonclassical Au(0)−CO complexes with physisorbed CO may be relevant to the surface IR data.

7. Conclusions

We report a combined experimental and theoretical study of a series of gas-phase di-gold carbonyl clusters, $Au_2(CO)_n^-$ ($n = 1−3$). Photoelectron spectroscopy shows that adsorption of the first two CO's each induces a significant red-shift in the electron binding energies (0.69 and 0.56 eV) and the third CO only induces a slight blue-shift (0.17 eV), indicating a chemisorption-to-physisorption transition from $n = 2$ to $n = 3$ in $Au_2(CO)_n^-$. The ground-state detachment transitions for $Au_2(CO)_2^-$ and $Au_2(CO)_3^-$ are vibrationally resolved, yielding vibrational frequencies of 2110 ± 40 and 2160 ± 40 cm^{-1} for the neutral $Au_2(CO)_2$ and $Au_2(CO)_3$ clusters, respectively. The $Au_2(CO)_3$ species represents a nonclassical Au(0)−CO complex and may be relevant to surface carbonyl species under high CO coverage. DFT calculations at the PW91 level are carried out to determine the structures of $Au_2(CO)_n^-$ and $Au_2(CO)_n$ ($n = 1−3$). Both $Au_2(CO)$ and $Au_2(CO)_2$ are found to be linear molecules with CO coordinated to Au terminally via C. However, $Au_2(CO)^-$ is found to be bent due to the Renner−Teller effect, whereas strong spin−orbit effects in $Au_2(CO)_2^-$ quench the Renner−Teller effect to remain linear. $Au_2(CO)_3^-$ is found to be a physisorbed complex, in which the third CO is only weakly interacting with a linear $Au_2(CO)_2^-$ core. Both pure GGA and hybrid DFT methods are found to be inadequate to predict the relative energies for the CO physisorption versus chemisorption in $Au_2(CO)_3^-$. CCSD(T) calculations have to be used, showing that the physisorption isomer is the ground state, in agreement with the experimental observation.

References and Notes

(1) For selected recent reviews, see: (a) Haruta, M. *Catal. Today* **1997**, *36*, 153. (b) Haruta, M. *Chem. Rec.* **2003**, *3*, 75. (c) Bond, G. C.; Thompson,

D. T. *Catal. Rev.-Sci. Eng.* **1999**, *41*, 319. (d) Meyer, R.; Lemire, C.; Shaikhutdinov, Sh. K.; Freund, H.-J. *Gold Bull.* **2004**, *37*, 72. (e) Kung, M. C.; Davis, R. J.; Kung, H. H. *J. Phys. Chem. C* **2007**, *111*, 11767.

(2) (a) Valden, M.; Lai, X.; Goodman, D. W. *Science* **1998**, *281*, 1647. (b) Chen, M. S.; Goodman, D. W. *Science* **2004**, *306*, 252. (c) Chen, M. S.; Kumar, D.; Yi, C. W.; Goodman, D. W. *Science* **2005**, *310*, 291.

(3) (a) Sanchez, A.; Abbet, S.; Heiz, U.; Schneider, W. D.; Häkkinen, H.; Barnett, R. N.; Landman, U. *J. Phys. Chem. A* **1999**, *103*, 9573. (b) Yoon, B.; Häkkinen, H.; Landman, U.; Wirz, A. S.; Antonietti, J. M.; Abbet, S.; Judai, K.; Heiz, U. *Science* **2005**, *307*, 403.

(4) (a) Kim, T. S.; Stiehl, J. D.; Reeves, C. T.; Meyer, R. J.; Mullins, C. B. *J. Am. Chem. Soc.* **2003**, *125*, 2018. (b) Stiehl, J. D.; Kim, T. S.; McClure, S. M.; Mullins, C. B. *J. Am. Chem. Soc.* **2004**, *126*, 1606.

(5) (a) Wahlstrom, E.; Lopez, N.; Schaub, R.; Thostrup, P.; Ronnau, A.; Africh, C.; Lægsgaard, E.; Norskov, J. K.; Besenbacher, F. *Phys. Rev. Lett.* **2003**, *90*, 026101. (b) Matthey, D.; Wang, J. G.; Wendt, S.; Matthiesen, J.; Schaub, R.; Lægsgaard, E.; Hammer, B.; Besenbacher, F. *Science* **2007**, *315*, 1692.

(6) Fu, Q.; Saltsburg, H.; Flytzani-Stephanopoulos, M. *Science* **2003**, *301*, 935.

(7) Guzman, J.; Gates, B. C. *J. Am. Chem. Soc.* **2004**, *126*, 2672.

(8) Date, M.; Okumura, M.; Tsubota, S.; Haruta, M. *Angew. Chem., Int. Ed.* **2004**, *43*, 2129.

(9) Lemire, C.; Meyer, R.; Shaikhutdinov, S.; Freund, H.-J. *Angew. Chem., Int. Ed.* **2004**, *43*, 118.

(10) Lee, S.; Fan, C.; Wu, T.; Anderson, S. L. *J. Am. Chem. Soc.* **2004**, *126*, 5682.

(11) Deng, X.; Min, B. K.; Guloy, A.; Friend, C. M. *J. Am. Chem. Soc.* **2005**, *127*, 9267.

(12) (a) Hughes, M. D.; Xu, Y. J.; Jenkins, P.; McMorn, P.; Landon, P.; Enache, D. I.; Carley, A. F.; Attard, G. A.; Hutchings, G. J.; King, F.; Stitt, E. H.; Johnston, P.; Griffin, K.; Kiely, C. J. *Nature* **2005**, *437*, 1132. (b) Enache, D. I.; Edwards, J. K.; Landon, P.; Solsona-Espriu, B.; Carley, A. F.; Herzing, A. A.; Watanabe, M.; Kiely, C. J.; Knight, D. W.; Hutchings, G. J. *Science* **2006**, *311*, 362. (c) Herzing, A. A.; Kiely, C. J.; Carley, A. F.; Landon, P.; Hutchings, G. J. *Science* **2008**, *321*, 1331.

(13) (a) Sterrer, M.; Yulikov, M.; Risse, T.; Freund, H.-J.; Carrasco, J.; Illas, F.; Di Valentin, C.; Giordano, L.; Pacchioni, G. *Angew. Chem., Int. Ed.* **2006**, *45*, 2633. (b) Sterrer, M.; Yulikov, M.; Fischbach, E.; Heyde, M.; Rust, H. P.; Pacchioni, G.; Risse, T.; Freund, H.-J. *Angew. Chem., Int. Ed.* **2006**, *45*, 2630.

(14) Hayden, B. E.; Pletcher, D.; Suchsland, J. P. *Angew. Chem., Int. Ed.* **2007**, *46*, 3530.

(15) Turner, M.; Golovko, V. B.; Vaughan, O. P. H.; Abdulkin, P.; Berenguer-Murcia, A.; Tikhov, M. S.; Johnson, B. F. G.; Lambert, R. M. *Nature* **2008**, *454*, 981.

(16) (a) Liu, Z. P.; Hu, P.; Alavi, A. *J. Am. Chem. Soc.* **2002**, *124*, 14770. (b) Liu, Z. P.; Gong, X. Q.; Kohanoff, J.; Sanchez, C.; Hu, P. *Phys. Rev. Lett.* **2003**, *91*, 266102. (c) Liu, Z. P.; Jenkins, S. J.; King, D. A. *Phys. Rev. Lett.* **2005**, *94*, 196102.

(17) Lopez, N.; Janssens, T. V. W.; Clausen, B. S.; Xu, Y.; Mavrikakis, M.; Bligaard, T.; Norskov, J. K. *J. Catal.* **2004**, *223*, 232.

(18) (a) Molina, L. M.; Hammer, B. *Phys. Rev. Lett.* **2003**, *90*, 206102. (b) Molina, L. M.; Hammer, B. *J. Chem. Phys.* **2005**, *123*, 161104. (c) Molina, L. M.; Lesarri, A.; Alonso, J. A. *Chem. Phys. Lett.* **2009**, *468*, 201.

(19) Cho, A. *Science* **2003**, *299*, 1684.

(20) Cox, D. M.; Brickman, R.; Creegan, K.; Kaldor, A. *Z. Phys. D* **1991**, *19*, 353.

(21) Lee, T. H.; Ervin, K. M. *J. Phys. Chem.* **1994**, *98*, 10023.

(22) Salisbury, B. E.; Wallace, W. T.; Whetten, R. L. *Chem. Phys.* **2000**, *262*, 131.

(23) (a) Stolcic, D.; Fischer, M.; Gantefor, G.; Kim, Y. D.; Sun, Q.; Jena, P. *J. Am. Chem. Soc.* **2003**, *125*, 2848. (b) Kim, Y. D.; Fischer, M.; Gantefor, G. *Chem. Phys. Lett.* **2003**, *377*, 170. (c) Sun, Q.; Jena, P.; Kim, Y. D.; Fischer, M.; Gantefor, G. *J. Chem. Phys.* **2004**, *120*, 6510.

(24) (a) Hagen, J.; Socaciu, L. D.; Elijazyfer, M.; Heiz, U.; Bernhardt, T. M.; Wöste, L. *Phys. Chem. Chem. Phys.* **2002**, *4*, 1707. (b) Socaciu, L. D.; Hagen, J.; Bernhardt, T. M.; Wöste, L.; Heiz, U.; Häkkinen, H.; Landman, U. *J. Am. Chem. Soc.* **2003**, *125*, 10437. (c) Hagen, J.; Socaciu, L. D.; Heiz, U.; Bernhardt, T. M.; Wöste, L. *Eur. Phys. J. D* **2003**, *24*, 327.

(25) Wallace, W. T.; Whetten, R. L. *J. Am. Chem. Soc.* **2002**, *124*, 7499.

(26) (a) Kimble, M. L.; Castleman, A. W., Jr.; Mitric, R.; Bürgel, C.; Bonacic-Koutecky, V. *J. Am. Chem. Soc.* **2004**, *126*, 2526. (b) Kimble, M.; Moore, N. A.; Johnson, G. E.; Castleman, A. W., Jr.; Bürgel, C.; Mitric, R.; Bonacic-Koutecky, V. *J. Chem. Phys.* **2006**, *125*, 204311. (c) Bürgel, C.; Reilly, N. M.; Johnson, G. E.; Mitric, R.; Kimble, M. L.; Castleman, A. W., Jr.; Bonacic-Koutecky, V. *J. Am. Chem. Soc.* **2008**, *130*, 1694. (d) Johnson, G. E.; Reilly, N. M.; Tyo, E. C.; Castleman, A. W., Jr. *J. Phys. Chem. C* **2008**, *112*, 9730.

(27) Veldeman, N.; Lievens, P.; Andersson, M. *J. Phys. Chem. A* **2005**, *109*, 11793.

(28) Zhai, H. J.; Bürgel, C.; Bonacic-Koutecky, V.; Wang, L. S. *J. Am. Chem. Soc.* **2008**, *130*, 9156.

(29) Nygren, M. A.; Siegbahn, P. E. M.; Jin, C.; Guo, T.; Smalley, R. E. *J. Chem. Phys.* **1991**, *95*, 6181.

(30) (a) Wallace, W. T.; Whetten, R. L. *J. Phys. Chem. B* **2000**, *104*, 10964. (b) Wallace, W. T.; Wyrwas, R. B.; Leavitt, A. J.; Whetten, R. L. *Phys. Chem. Chem. Phys.* **2005**, *7*, 930.

(31) Liang, B.; Andrews, L. *J. Phys. Chem. A* **2000**, *104*, 9156.

(32) Luttgens, G.; Pontius, N.; Bechthold, P. S.; Neeb, M.; Eberhardt, W. *Phys. Rev. Lett.* **2002**, *88*, 076102.

(33) Balteanu, I.; Balaj, O. P.; Fox, B. S.; Beyer, M. K.; Bastl, Z.; Bondybey, V. E. *Phys. Chem. Chem. Phys.* **2003**, *5*, 1213.

(34) (a) Jiang, L.; Xu, Q. *J. Phys. Chem. A* **2005**, *109*, 1026. (b) Xu, Q.; Jiang, L. *J. Phys. Chem. A* **2006**, *110*, 2655.

(35) (a) Fielicke, A.; von Helden, G.; Meijer, G.; Pedersen, D. B.; Simard, B.; Rayner, D. M. *J. Am. Chem. Soc.* **2005**, *127*, 8146. (b) Fielicke, A.; von Helden, G.; Meijer, G.; Simard, B.; Rayner, D. M. *J. Phys. Chem. B* **2005**, *109*, 23935.

(36) (a) Neumaier, M.; Weigend, F.; Hampe, O.; Kappes, M. M. *J. Chem. Phys.* **2005**, *122*, 104702. (b) Neumaier, M.; Weigend, F.; Hampe, O.; Kappes, M. M. *J. Chem. Phys.* **2006**, *125*, 104308. (c) Neumaier, M.; Weigend, F.; Hampe, O.; Kappes, M. M. *Faraday Discuss.* **2008**, *138*, 393.

(37) Velasquez, J., III.; Njegic, B.; Gordon, M. S.; Duncan, M. A. *J. Phys. Chem. A* **2008**, *112*, 1907.

(38) Häkkinen, H.; Landman, U. *J. Am. Chem. Soc.* **2001**, *123*, 9704.

(39) Wu, X.; Senapati, L.; Nayak, S. K.; Selloni, A.; Hajaligol, M. *J. Chem. Phys.* **2002**, *117*, 4010.

(40) Yuan, D. W.; Zeng, Z. *J. Chem. Phys.* **2004**, *120*, 6574.

(41) Schwerdtfeger, P.; Lein, M.; Krawczyk, R. P.; Jacob, C. R. *J. Chem. Phys.* **2008**, *128*, 124302.

(42) (a) Varganov, S. A.; Olson, R. M.; Gordon, M. S.; Meitu, H. *J. Chem. Phys.* **2003**, *119*, 2531. (b) Varganov, S. A.; Olson, R. M.; Gordon, M. S.; Mills, G.; Meitu, H. *Chem. Phys. Lett.* **2003**, *368*, 778. (c) Mills, G.; Gordon, M. S.; Meitu, H. *Chem. Phys. Lett.* **2002**, *359*, 493.

(43) Yoon, B.; Häkkinen, H.; Landman, U. *J. Phys. Chem. A* **2003**, *107*, 4066.

(44) (a) Ding, X. L.; Li, Z. Y.; Yang, J. L.; Hou, J. G.; Zhu, Q. S. *J. Chem. Phys.* **2004**, *120*, 9594. (b) Ding, X. L.; Dai, B.; Yang, J. L.; Hou, J. G.; Zhu, Q. S. *J. Chem. Phys.* **2004**, *121*, 621.

(45) McKenna, K. P.; Shluger, A. L. *J. Phys. Chem. C* **2007**, *111*, 18848.

(46) Mitric, R.; Bürgel, C.; Bonacic-Koutecky, V. *Proc. Natl. Acad. Sci. U.S.A.* **2007**, *104*, 10314.

(47) Prestianni, A.; Martorana, A.; Ciofini, I.; Labat, F.; Adamo, C. *J. Phys. Chem. C* **2008**, *112*, 18061.

(48) Torres, M. B.; Fernandez, E. M.; Balbas, L. C. *J. Phys. Chem. A* **2008**, *112*, 6678.

(49) (a) An, W.; Pei, Y.; Zeng, X. C. *Nano Lett.* **2008**, *8*, 195. (b) Gao, Y.; Shao, N.; Bulusu, S.; Zeng, X. C. *J. Phys. Chem. C* **2008**, *112*, 8234.

(50) Zhai, H. J.; Wang, L. S. *J. Chem. Phys.* **2005**, *122*, 051101.

(51) Zhai, H. J.; Kiran, B.; Dai, B.; Li, J.; Wang, L. S. *J. Am. Chem. Soc.* **2005**, *127*, 12098.

(52) Zhai, H. J.; Pan, L.-L.; Dai, B.; Kiran, B.; Li, J.; Wang, L. S. *J. Phys. Chem. C* **2008**, *112*, 11920.

(53) Worz, A. S.; Heiz, U.; Cinquini, F.; Pacchioni, G. *J. Phys. Chem. B* **2005**, *109*, 18418.

(54) Yates, D. J. C. *J. Colloid Interface Sci.* **1969**, *29*, 194.

(55) Lee, J. Y.; Schwank, J. *J. Catal.* **1986**, *102*, 207.

(56) Guillemot, D.; Borovkov, V. Yu.; Kazansky, V. B.; Polisset-Thfoin, M.; Fraissard, J. *J. Chem. Soc., Faraday Trans.* **1997**, *93*, 3587.

(57) Lemire, C.; Meyer, R.; Shaikhutdinov, S. K.; Freund, H.-J. *Surf. Sci.* **2004**, *552*, 27.

(58) Centeno, M. A.; Hadjiivanov, K.; Venkov, Tz.; Klimev, Hr.; Odriozola, J. A. *J. Mol. Catal. A* **2006**, *252*, 142.

(59) Tadayyoni, M. A.; Weaver, M. J. *Langmuir* **1986**, *2*, 179.

(60) Boccuzzi, F.; Chiorini, A.; Tsubota, S.; Haruta, M. *J. Phys. Chem.* **1996**, *100*, 3625.

(61) Maciejewski, M.; Fabrizioli, P.; Grunwaldt, J. D.; Becker, O. S.; Baiker, A. *Phys. Chem. Chem. Phys.* **2001**, *3*, 3846.

(62) Karpenko, A.; Leppelt, R.; Plzak, V.; Behm, R. J. *J. Catal.* **2007**, *252*, 231.

(63) (a) Wang, L. S.; Cheng, H. S.; Fan, J. *J. Chem. Phys.* **1995**, *102*, 9480. (b) Wang, L. S.; Wu, H. In *Advances in Metal and Semiconductor Clusters. IV. Cluster Materials*; Duncan, M. A., Ed.; JAI Press: Greenwich, CT, 1998; pp 299−343.

(64) ADF 2007.01, SCM, Theoretical Chemistry, Vrije Universiteit, Amsterdam, The Netherlands (http://www.scm.com). (a) te Velde, G.; Bickelhaupt, F. M.; Baerends, E. J.; Guerra, C. F.; van Gisbergen, S. J. A.; Snijders, J. G.; Ziegler, T. *J. Comput. Chem.* **2001**, *22*, 931. (b) Guerra, C. F.; Snijders, J. G.; te Velde, G.; Baerends, E. J. *Theor. Chem. Acc.* **1998**, *99*, 391.

(65) van Lenthe, E.; Baerends, E. J. *J. Comput. Chem.* **2003**, *24*, 1142.

(66) van Lenthe, E.; Baerends, E. J.; Snijders, J. G. *J. Chem. Phys.* **1993**, *99*, 4597.

1254 *J. Phys. Chem. A, Vol. 114, No. 3, 2010*

Wang et al.

(67) Li, J.; Li, X.; Zhai, H. J.; Wang, L. S. *Science* **2003**, *299*, 864.

(68) (a) Purvis, G. D.; Bartlett, R. J. *J. Chem. Phys.* **1982**, *76*, 1910. (b) Scuseria, G. E.; Janssen, C. L.; Schaefer, H. F. *J. Chem. Phys.* **1988**, *89*, 7382.

(69) Werner, H.-J.; *MOLPRO, version 2008.1, a package of ab initio programs*; see: http://www.molpro.net.

(70) Figgen, D.; Rauhut, G.; Dolg, M.; Stoll, H. *Chem. Phys.* **2005**, *311*, 227.

(71) Peterson, K. A.; Puzzarini, C. *Theor. Chem. Acc.* **2005**, *114*, 283.

(72) Dunning, T. H., Jr. *J. Chem. Phys.* **1989**, *90*, 1007.

(73) Berning, A.; Schweizer, M.; Werner, H.-J.; Knowles, P. J.; Palmieri, P. *Mol. Phys.* **2000**, *98*, 1823.

(74) (a) Roos, B. O.; Taylor, P. R.; Siegbahn, P. E. M. *Chem. Phys.* **1980**, *48*, 157. (b) Roos, B. O. *Int. J. Quantum Chem.* **1980**, *S14*, 175.

(75) Bylaska, E. J.; *NWChem, A Computational Chemistry Package for Parallel Computers, Version 5.0*; Pacific Northwest National Laboratory, Richland, WA 99352-0999, 2006.

(76) Boys, S. F.; Bernardi, F. *Mol. Phys.* **1970**, *19*, 553.

(77) Zhai, H. J.; Kiran, B.; Wang, L. S. *J. Chem. Phys.* **2004**, *121*, 8231.

(78) Ho, J.; Ervin, K. M.; Lineberger, W. C. *J. Chem. Phys.* **1990**, *93*, 6987.

(79) Dreuw, A.; Weisman, J. L.; Head-Gordon, M. *J. Chem. Phys.* **2003**, *119*, 2943.

(80) Bagus, P. S.; Pacchioni, G. *J. Phys. Conf. Ser.* **2008**, *117*, 012003.

(81) Giordano, L.; Carrasco, J.; Di Valentin, C.; Illas, F.; Pacchioni, G. *J. Chem. Phys.* **2006**, *124*, 174709.

(82) Renner, R. *Z. Phys.* **1934**, *92*, 172.

(83) Pan, L. L.; Li, J.; Wang, L. S. *J. Chem. Phys.* **2008**, *129*, 024302.

(84) (a) Rack, J. J.; Strauss, S. H. *Catal. Today* **1997**, *36*, 99. (b) Strauss, S. H. *J. Chem. Soc., Dalton Trans.* **2000**, 1.